Catalysis Today 224 (2014) 122–131

Contents lists available at ScienceDirect

Catalysis Today

journal homepage: www.elsevier.com/locate/cattod

Photodegradation of contaminants using Ag@AgCl/rGO assemblages: Possibilities and limitations

Huijie Yu[a], Christopher J. Miller[a], Atsushi Ikeda-Ohno[a,b], T. David Waite[a,*]

[a] School of Civil and Environmental Engineering, The University of New South Wales, Sydney, NSW 2052, Australia
[b] Institute for Environmental Research Australian Nuclear Science and Technology Organisation Locked Bag 2001, Kirrawee DC, NSW 2232, Australia

ARTICLE INFO

Article history:
Received 3 August 2013
Received in revised form 28 October 2013
Accepted 2 December 2013
Available online 29 December 2013

Keywords:
Ag@AgCl
Reduced graphene oxide
Reactive oxygen species
Visible light irradiation
Formic acid degradation
Plasmonic photocatalysis

ABSTRACT

Plasmonic photocatalysts of the form Ag@AgCl/rGO were synthesized by a deposition–precipitation–photoreduction method and the composite materials characterized using Raman spectroscopy, attenuated total reflection-Fourier transform infrared spectroscopy (ATR-FTIR), X-ray photoelectron spectroscopy (XPS) and X-ray absorption spectroscopy (XAS), scanning electron microscopy (SEM) and transmission electron microscopy (TEM). The as-prepared plasmonic photocatalysts exhibited enhanced photoactivity for the degradation of formic acid (FA) under visible light irradiation, however, both the Ag@AgCl and the graphene oxide support underwent continuous transformation during photolysis. The high activity was attributed principally to the ability of the composite Ag^0/AgCl system to absorb light in the visible wavelength region and to retard the recombination of electron–hole pairs. While the presence of the reduced graphene oxide (rGO) support may also have contributed to a reduction in rate of electron–hole pair recombination, the effect was not found to be particularly significant. HO• trapping experiments with phthalhydrazide as well as the influence of *t*-butanol on FA degradation suggested that either photo-formed holes or surface chlorine atoms were the main reactive species inducing degradation of FA under visible light irradiation. Total free chlorine, but not hydrogen peroxide, could be detected by *N*,*N*-diethyl-*p*-phenylenediamine (DPD) spectrophotometry suggesting that while photogenerated holes decay via reaction with chloride ions, photogenerated electrons decay via a pathway other than reaction with oxygen. Possible reaction mechanisms that conform to these observations are discussed. Although this system has potential for the oxidative degradation of contaminants, greater understanding of the factors that promote excessive Ag(I) reduction, concomitant formation of Ag(0) and eventual deactivation of the catalyst is needed.

1. Introduction

Semiconductor photocatalysis has attracted increasing interest as a promising technique for contaminant remediation, clean fuel generation and global warming amelioration [1,2]. However, since the photo-electrochemical splitting of water on *n*-TiO_2 electrodes was discovered [3], most of the semiconductor materials still suffer from insufficient visible light response and fast recombination of photogenerated carriers. The use of visible light driven photocatalysts for the degradation of contaminants is particularly desirable as it enables the use of freely available solar irradiation, leading to cost-effective processes [4].

Silver halides (AgX), although well-known photographic materials, have only recently been investigated as so-called stable photocatalysts. Following the work of Calzaferri et al. on the use of silver chloride as a photoanode material for water splitting [5,6], Huang et al. reported that Ag@AgCl photocatalysts exhibited reasonable stability and efficient photocatalytic activity for degradation of organic dyes [7]. Subsequently, there has been a remarkable upsurge in use of AgX as photocatalysts, usually either coupled with plasmonic metallic Ag (Ag@AgX), produced as composites with various halides or supported on active or inactive materials [8]. There has been particular recent exploration in improving the durability, efficiency and activity of AgX by enhancing the separation of photogenerated charge carriers and introducing synergistic effects through use of cost effective and versatile supports for these small band-gap semiconducting materials.

Graphene and graphene derivatives such as graphene oxide (GO) and reduced graphene oxide (rGO) have attracted particular interest as support materials in recent years [9–11]. Graphene-based nanocomposites have shown excellent performance in optical, electrical and catalytic fields as a result not only of the high mobility of electrons within these one atom thick sp^2-bonded carbon sheets, but also because of the ability of these materials

* Corresponding author. Tel.: +61293855060.
E-mail address: d.waite@unsw.edu.au (T.D. Waite).

0920-5861/$ – see front matter © 2013 Elsevier B.V. All rights reserved.
http://dx.doi.org/10.1016/j.cattod.2013.12.005

to modulate the electronic structure of anchored metal and non-metal nanocrystals. These desirable features are augmented with oxygen-bearing groups (such as carboxylic, carbonyl and hydroxyl groups) within the structure which provide both good dispersibility and reactive sites for the nucleation and growth of photocatalyst particles, with both GO and rGO previously found to significantly improve the performance of Ag@AgX composites [12–18].

It is generally acknowledged that the reactive oxidizing species (such as holes or hydroxyl radicals ($HO^{\bullet}$)) involved in the photocatalysis process depends not only on the particular catalyst used but also on the nature of the support (if any) and the specific species undergoing degradation [4,19]. Although almost all previous studies utilizing AgX as visible light driven photocatalysts have demonstrated the activity and stability of these materials for the decomposition of organic pollutants, neither the mechanistic aspects of these reactions have been provided [16,17,20] nor the factors important to optimizing the photocatalytic process elucidated adequately [21,22].

While dyes have been used widely as target species in oxidation studies, their use in light-mediated degradation investigations is problematic as the dye itself suffers from self-sensitization and may undergo other specific photochemical processes that are dependent upon the nature of the dye and the semiconductor, thus leading to poor generality of the results obtained [23]. To the best of our knowledge, there are no evaluations on the degradation of other refractory intermediates such as aliphatic acids (formic acid, acetic acid, oxalic acid, etc.) using AgX based photocatalysts, which is important for total mineralization of organic contaminants. As such, we have chosen to use formic acid (FA) as the target compound in these studies as it does not absorb visible light (thus enabling evaluation of the photocatalyst performance), oxidizes to CO_2 [24,25] and has been used previously as a hole scavenger and probe compound in photocatalytic degradation studies [26–29].

2. Experimental

2.1. Regents, materials and apparatus

Sodium formate (ACS reagent, 99+%) was from Acros, silver nitrate was from Ajax Inc. and ammonium hydroxide (28%), hydrochloric acid (32%), sodium formate-^{14}C and ethanol (200 proof, HPLC/Spectrophotometric grade) were from Sigma-Aldrich. Graphite (SP–1, spectroscopic powders) was supplied by Bay Carbon Inc. All other reagents were at least of analytical reagent grade and used without further purification. All solutions were prepared in 18 MΩ cm water (MQ) from a Millipore Milli-Q system. Stock solutions were kept in dark bottles, covered in foil and refrigerated at 4 °C when not in use. All solutions were prepared in 10 mM NaCl buffered by 2.0 mM $NaHCO_3$ (or as otherwise stated), with the pH adjusted to 8.0 with 1 M $HClO_4$ or NaOH.

All glassware and plasticware were soaked in 5% w/v HNO_3 for at least 1 week before use. For free chlorine and hydrogen peroxide analysis, all glassware was soaked with 19 g of ammonium persulfate (ACS reagent, 98%) in two litres of 98% sulfuric acid (AR, Ajax) for 1 week, soaked with 1 mM sodium hypochlorite (6–14% active chlorine basis, Sigma-Aldrich), and then further thoroughly washed with 18 MΩ cm water. All working solutions of sodium hypochlorite and hydrogen peroxide were prepared freshly.

A 300 W Xenon arc lamp (PLS-SXE300, Beijing Perfectlight Technology Co., Ltd) equipped with a UV-cutoff filter ($\lambda > 400$ nm) was used as the light source in all studies. Light from this source passed through a 10 cm water filter positioned 10 cm from the reactor before overhead irradiation of the reactant solution.

2.2. Ag@AgCl/rGO preparation

(GO) was prepared by a modified Tour's method and Ag@AgCl/rGO assemblages subsequently prepared using a deposition–precipitation–photoreduction process that is described in detail elsewhere [30]. The preparation of the photocatalyst includes a photoreduction step in 50% ethanol under argon with the catalysts, on the basis of the duration of this photoreduction period (30, 60, 90, 120, 160, 200 and 240 min), denoted as XAg@AgCl/rGO (where X = 30–240). For comparison purposes, an AgCl/GO assemblage exposed only to indoor light was prepared by excluding the Xenon lamp irradiation step (denoted as 0Ag@AgCl/rGO). Ag@AgCl with 30 min photoreduction time (denoted as 30Ag@AgCl) was prepared in a similar manner to Ag@AgCl/rGO but without GO as support with only a 30 min photoreduction period employed as longer duration irradiations were observed to lead to significant aggregation of metallic silver.

To test the stability and reusability of the catalysts, the 90Ag@AgCl/rGO catalyst was utilized in a FA oxidation experiment and then recovered with centrifugation after 40 min, 90 min, 120 min and 180 min, denoted as 90Ag@AgCl/rGOY(where Y = 40, 90, 120, 180), respectively.

2.3. Characterization of the catalysts

Various techniques were used to characterize the photocatalyst particles, as described below.

Fourier transform infrared spectroscopy (FTIR) was carried out with Spotlight 400 and Spectrum 100 (Perkin Elmer) instruments equipped with an attenuated total reflection (ATR) accessory. Four scans with 4 cm^{-1} resolution per sample were recorded between 4000 and 650 cm^{-1}.

Raman spectroscopy was performed on an inVia Renishaw Raman microscope using a 514.5 nm argon laser excitation with 0.5% of laser power to minimize the laser damage. Scans were taken in static mode (999–1862 cm^{-1}) and the exposure time was 10 s for the green laser. The spot diameter was ~2 μm with a 50× objective lens. The calibration was undertaken using an internal silicon reference at 520 cm^{-1}.

The surface composition and chemical states of the samples were analysed by X-ray photoelectron spectroscopy (XPS) using an ESCALAB250Xi instrument with a 200 W (20 mA and 10 kV) monochromatic Al *K*α source (energy 1486.6 eV) and with a vacuum better than 2×10^{-9} mbar. The sample spot was approximately 500 μm in cross section with a photoelectron takeoff angle of 90° and pass energy of 100 eV for survey scans or 20 eV for surface region scans having step sizes of 0.5 eV for survey scans or 0.1 eV for region scans. The XPS spectra of the samples were deconvoluted by Thermo Scientific Advantage software (version 4.7.4) after performing a Shirley background correction. Calibration was performed by alignment of the spectra with reference to the C 1s line at 284.8 ± 0.2 eV associated with graphitic carbon. The XPS peaks were fitted to Voigt functions having mixed Gaussian and Lorentzian character.

X-ray absorption spectroscopy including X-ray absorption near-edge structure (XANES) and extended X-ray absorption fine structure (EXAFS) was employed to determine the oxidation states and speciation of Ag in the samples. Ag *K*-edge X-ray absorption spectra were collected on the XAS beamline at the Australian Synchrotron under the ring operating condition of 3 GeV (top-up mode). A Si(311) double crystal was employed to obtain monochromatic X-rays from the synchrotron. The spectra were collected in transmission mode using N_2—filled ionization chambers. The measurements were performed in vacuum at 6 K. Reference samples of Ag metal and AgCl were also measured in transmission mode. The energy of each spectrum was corrected on the first inflection

point of Ag metal foil (25.5140 keV) which was measured simultaneously with the samples. The collected absorption spectra were treated according to a standard procedure [31] using the program WinXAS (version 3.2) [32]. Linear combination fitting (LCF) analysis was performed on EXAFS spectra using the same software.

The specific surface areas (SSA) of the as-prepared catalysts were measured on a Micromeritics Tristar 3000 by nitrogen adsorption at 77 K and analysed using the Brunauer–Emmett–Teller (BET) isotherm. Temperature programmed reduction and desorption experiments were performed on a Micromeritics Autochem 2920.

The morphology and size of the resultant products were observed using a scanning electron microscope (SEM, Hitachi S3400-I) under secondary electron (SE) mode at accelerating voltage of 15 kV with a probe current of 30 mA and working distance of 10 mm The specimen was prepared by spreading powder onto a carbon grid, sputter-coated with a ~10 nm thick layer of conductive chromium with Emitech K575x Chromium Sputter Coater and followed by overnight drying in a vacuum oven at 35 °C.

In order to clearly investigate the interfaces among Ag, AgCl and rGO, the structure of the Ag@AgCl/rGO was further characterized by transmission electron microscopy (TEM, Philips CM200) at an accelerating voltage of 200 kV. The specimen was prepared by dropping the dispersed powder solution onto a copper grid coated with amorphous carbon and dried naturally.

2.4. Photocatalytic reactivity studies

All photocatalytic degradation runs were performed under atmospheric conditions in a magnetically stirred 250 mL cylindrical Pyrex reactor with temperature maintained at 25 ± 1 °C by placing the reactor in a temperature controlled water bath. In order to avoid the complete consumption of oxygen during photocatalysis, high purity air was constantly bubbled through the suspension at a flowrate of 0.5 L min^{-1}. All reactions were undertaken in solutions containing 10 mM NaCl and 2 mM $NaHCO_3$ which, in equilibrium with atmospheric CO_2, were reasonably buffered at pH 8.0 ± 0.1.

2.4.1. ^{14}C-labelled sodium formate degradation

In a typical experiment, appropriate volumes of 100 μM "cold" sodium formate, 100 nM ^{14}C-labelled sodium formate and 50 mg of Ag@AgCl/rGO were added to the $NaHCO_3$/NaCl solution with the final volume made up to 100 mL. Control experiments were undertaken and demonstrated that Ag@AgCl/rGO did not degrade FA in the dark.

Prior to the irradiation, the suspensions were magnetically stirred in the dark for 30 min to achieve adsorption–desorption equilibrium of the substrate on the photocatalyst surface, with stirring continued during the runs. At selected time intervals, 2 mL aliquots of the suspension were withdrawn from the reactor and the photocatalyst separated from the solution by centrifugation at 4000 rpm for 5 min. 1 mL of the supernatant was spiked into 4 mL of pH 2.9 $HClO_4$ solution. The mixture was thoroughly sparged with argon for at least 2 min to remove any residual radioactive $^{14}CO_2$ and then 1 mL of this solution diluted into 5 mL of high flash-point cocktail (Ultima GOLD, PACKARD) and analyzed for residual ^{14}C-labelled FA using a Packard Tri-Carb 2100TR scintillation counter. The actual residual FA concentration was determined by multiplication of the known ratio of "cold" to labelled FA. All kinetic runs were conducted at least twice in order to determine the experimental error associated with the procedure. Experiments in the presence of *t*-butanol (TBA) were conducted similarly.

2.4.2. HO• production measurements using phthalhydrazide

HO• production was investigated by addition of phthalhydrazide (Phth) according to Miller et al. [33], with experiments proceeding similarly to the formate work. Solution composition was 0.5 mM Phth, 10 mM NaCl, 2 mM $NaHCO_3$ with 0.5 g L^{-1} Ag@AgCl/rGO catalyst. The suspension was stirred in the dark for 30 min to achieve equilibrium prior to irradiation, with samples withdrawn as required, filtered through PVDF filters (0.22 μm, Millipore) and then analysed for hydroxylated phthalhydrazide (5-HO-Phth). Control experiments (described in detail in the Supporting Information) confirmed that 5-HO-Phth could be recovered from the solution, if it was indeed formed.

2.4.3. $HOCl/OCl^-$ and H_2O_2 measurements

Similar to the photodegradation experiments, 1 g L^{-1} of photocatalyst 90Ag@AgCl/rGO was stirred in the dark for 30 min and then irradiated by the Xenon light source. At different time intervals, 6 mL of the suspension was taken out, filtered in about 30 s through a Fluoropore PTFE membrane (0.22 μm, Millipore) and the first 0.5 mL of filtrate was discarded. 4.5 mL of filtrate was transferred into a quartz cell (5 cm, Starna), 0.5 mL of PO_4 buffer (0.25 M Na_2HPO_4 and 0.25 M NaH_2PO_4) and 50 μL of DPD solution (2.0 g L^{-1} DPD in 0.1 N H_2SO_4) rapidly added and the sample mixed for another 30 s. The absorption spectrum from 200 to 800 nm was then recorded for 1 min in kinetic mode using a Cary 50 spectrophotometer. The absorption at ~551 nm (after background correction) was due to the oxidation of DPD by $HOCl/OCl^-$ to form $DPD^{\bullet+}$. The background absorption was obtained by repeating the procedure with all reagents except DPD with the absorbance measured after filtration to remove the catalyst particles and addition into PO_4 buffer (but without DPD addition). After HOCl measurement, 50 μL of horseradish peroxidise (HRP) solution (20.0 kU L^{-1}) was then quickly added and the sample mixed. The increase in absorption (relative to that prior to addition of HRP) at ~551 nm was then determined, with this increase attributed to hydrogen peroxide.

3. Results and discussion

3.1. Microstructures of Ag@AgCl/rGO heterostructure

To understand the structural properties of the graphene materials, ATR–FTIR spectra were collected (see Supporting information Fig. S1). Graphene oxide exhibited peaks corresponding to the O–H stretching mode (~3400 cm^{-1}), C–OH vibrational mode (~1200 and 1050 cm^{-1}), C=C stretching (~1600 cm^{-1}), C=O vibrational mode (1750 cm^{-1}), O–C=O (1650–1750 cm^{-1}) and C–O–C/ether from epoxy groups (1000–1280 cm^{-1}). Upon photoreduction, the characteristic peak intensities from oxygen-bearing carbon groups decreased markedly, indicating that moderate reduction of GO to rGO occurred during the simultaneous transformation of AgCl to Ag nanoparticles on visible light irradiation. Similar spectra have been observed in previous FTIR studies of AgX/graphene composites [18]. The results obtained indicated that limited quantitative information on changes in nature of the graphene support on irradiation could be obtained by FTIR in view of the low content of graphene material and the comparatively lower content of oxygen functional groups present in the catalysts.

Raman spectroscopy has been widely used to characterize carbon materials because the spectra of these materials provide abundant information on crystallite size, crystal disorder, degree of hybridization, and extent of chemical modification [34–36]. The Raman spectra of all the photocatalyst samples were deconvoluted into five peaks with two Voigt contours (3L + 2V model) over the 999–1862 cm^{-1} range (see, for example, SI Fig. S2) [35]. In particular, the D band (~1350 cm^{-1}) is attributed to a breathing mode of κ-point phonons of A_{1g} symmetry, which is a common feature of sp^3 defects in carbon and is usually associated with the presence of structural defects, amorphous carbon, or edges that break the symmetry and selection rule while the G band (~1580 cm^{-1}) corresponds to the first-order scattering of the E_{2g} mode observed

for sp^2 carbon domains, which exists as the only Raman active peak in crystalline graphite. Band 1, with peak at ~1120 cm^{-1}, is associated with transpolyacetylene-like structures which are formed at the zigzag edges, the band centred at ~1536 cm^{-1} (the D″ band) is related with amorphous carbon or odd membered ring structure in graphitic compounds while the band at ~1620 cm^{-1} (the D′ band) is associated with isolated double bonds in highly oxidized GO [34–36]. The intensity ratio of the D band to the G band (I_D/I_G) is commonly used as an indicator of the extent of disorder and defects in graphene.

Compared with GO (I_D/I_G = 1.66) and the indoor light irradiated catalyst, 0Ag@AgClrGO (I_D/I_G = 1.99), the rGO produced through photoreduction exhibited a slightly lower I_D/I_G ratio of about 1.5. This could possibly be attributed to the increased disorder associated with the presence of oxygen defects, and/or the increase of smaller and dispersed sp^2 carbon moieties, although degradation of the reduced graphene oxide at long irradiation times could not be excluded [37]. Similar behaviour, that is, a small decrease or no change in I_D/I_G, has been observed in several previous studies [18,35,38].

XPS data also support both the conclusion that GO is highly-oxidized and that the abundant functional groups undergo continuous transformation on irradiation. While the relative levels of oxidation and transformation of groups during irradiation is of interest, the atomic C/O ratio could not be used for this purpose because it is difficult to fully dehydrate a GO sample (i.e., water is a significant contributor to the O peaks). Although there is considerable vagueness and subjectiveness to C 1s peak assignments, the deconvoluted peaks centred at the binding energy at 285, 286–286.4, ~287, 287.8–288, 289–289.4 eV were attributed to nonoxygenated graphitic C atoms (C=C, C–C, and C–H), hydroxyl group (C–OH), epoxy/ether groups (C–O–C), carbonyl (C=O) and carboxyl groups (O=C–OH), respectively [34,37,39]. The degree of GO reduction was monitored by the O-bound carbon content, which was estimated by dividing the areas under oxygenated C peaks by the sum of the areas under all C 1s peaks (Table 1). The C 1s XPS spectra were then normalized with respect to the nonoxygenated graphitic C peak (SI Fig. S3). It is likely that the variations in the distribution of C–O functional types reflects the difficulty of fitting so many oxygen-containing carbon peaks to the XPS spectra, which has only two clearly resolved peaks, as opposed to reflecting any actual C–O functional group changes. Although the individual oxygen-containing carbon peak components are ill-resolved, the summation of these peaks is still considered to be reasonably well-constrained.

It was found that the oxygenated functional groups (such as epoxide, carbonyl and carboxyl) transformed significantly and C=C bonds (sp^2 π-conjugated domains) formed in accord with reports in the literature [34,40,41]. GO as the graphene precursor contained 67% oxygenated carbon and 33% graphitic carbon, revealing highly effective oxidation of the commercial graphite. Visible light mediated photoreduction of GO and AgCl resulted in partial sp^2 graphitization in GO with significant variation in stoichiometric ratio between the functional moieties, while the O-bound carbon contents remained almost constant at 50 ± 4% (see Fig. 1). During the course of a FA degradation experiment, the O-bound carbon content was observed to significantly decrease, demonstrating continuous transformation of the rGO support during this process (Fig. 1 and Table 1)

From the silver XPS spectra of 90Ag@AgCl/rGO (see Supporting Information Fig. S4), two bands of silver were observed at binding energies at ~373.5 eV and ~367.5 eV and were ascribed to Ag 3d 3/2 and Ag 3d 5/2. The Ag peak of Ag 3d5/2 was deconvoluted into 367.5 eV and 368.5 eV components. The peak at ~367.5 eV could be attributed to monovalent Ag (AgCl), while the peak at ~368.5 eV could be attributed to metallic Ag, confirming that Ag^+ ions were

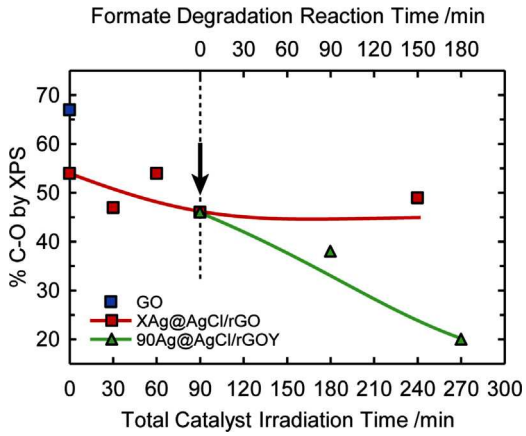

Fig. 1. Variation in oxygen-bound carbon as determined by XPS as a function of the catalyst irradiation time. Data is shown for the as prepared graphene oxide (GO), the photoreduced (under argon in 50% ethanol) XAg@AgCl/rGO catalyst (where "X" denotes the photoreduction radiation time) and also for 90Ag@AgCl/rGO photocatalyst recovered after degradation of FA ($[FA]_0$ = 100 μM, in pH 8, 10 mM NaCl, 2 mM $NaHCO_3$ buffer under air) after Y min irradiation in the presence of FA (90Ag@AgCl/rGOY, Y = 90, 180 min). Symbols are experimental data with lines for illustrative purposes only.

successfully reduced to metallic Ag. However, the disparate intensities and similar binding energy of these two peaks rendered the deconvolution process highly subjective such that the Ag^0 content could not be quantitatively determined by XPS. Therefore, in view of the low loading of graphene and the difficulty in quantifying the amount of Ag^0 present, XPS provided quite limited information on the changes that occurred in the hybrid AgCl/GO material during the photoreduction process.

Linear combination fitting (LCF) analysis reveals that the EXAFS spectra of the samples are composed of two oscillation components, that is, AgCl and metallic Ag. The atomic ratios of Ag^I (assumed to be present as Ag^ICl) and metallic Ag estimated by LCF are illustrated in Fig. 2 (and also summarised in SI Table S1). Ag *K*-edge EXAFS spectra for Ag@AgCl/rGO samples are dominated by that of AgCl (see SI Fig. S5). Extensive visible light irradiation reduced AgCl to metallic Ag with an increase in proportion of Ag^0 as irradiation time increased. For example, 240 min photoreduction of AgCl on GO resulted in the production of 8.42% of Ag^0, which was one order of magnitude greater than that produced by 60 min

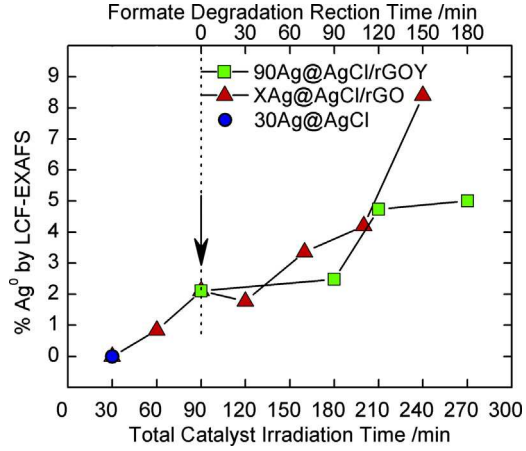

Fig. 2. Results from the LCF analysis of Ag *K*-edge EXAFS spectra. The triangles show the Ag(0) content of the as-prepared Ag@AgCl/rGO catalyst, with the squares showing the Ag(0) content of the 90 min irradiated Ag@AgCl/rGO catalyst after being used in a formate degradation experiment of duration shown by the upper time axis. The circle shows the Ag@AgCl catalyst, In all cases the lower time axis is the total period the catalyst has been irradiated (either in the presence or absence of formate).

Table 1
XPS, Raman and BET analysis for GO and Ag@AgCl/rGO photocatalyst.

	C=C, C–C, C–H (%)	C–OH (%)[a]	C–O–C (%)[a]	O=C (%)[a]	O=C–OH (%)[a]	O-bound carbon content (%)[a]	%Ag^0 (XPS)[b]	I_D/I_G	BET surface area ($m^2\ g^{-1}$)
GO	33	0	53	6	9	67	N/A	1.66	
30Ag@AgCl									0.62
0Ag@AgCl/rGO	46	0	39	9	6	54	12.7	1.93	
30Ag@AgCl/rGO	52	14	0	27	6	47	5.1	1.43	1.82
60Ag@AgCl/rGO	46	17	0	30	6	54	5.7	1.35	1.58
90Ag@AgCl/rGO	53	0	41	0	5	46	9.0	1.35	2.25
160Ag@AgCl/rGO									1.87
200Ag@AgCl/rGO									1.23
240Ag@AgCl/rGO	51	0	44	0	5	49	3.8	1.48	
90Ag@AgCl/rGO90	61	13	0	18	7	38	100	1.54	
90Ag@AgCl/rGO180	80	11	0	6	3	20	100	1.43	

[a] There is a high degree of uncertainty inherent with the C 1s deconvolution process that renders the estimates for individual C–O functionalities to be highly circumspect, however, the summation of these components is well defined (as the C 1s spectra clearly has two peaks), such that the estimate for O-bound carbon is quite well constrained.
[b] Due to the overlap of the Ag(0) and Ag(I) XPS peaks there is significant uncertainty in the % Ag^0 content, as this peak is merely an ill-defined, low intensity shoulder. The Ag^0 content from XPS is merely given for completeness and is not reliable.

photoreduction of AgCl on GO. A similar trend of Ag^ICl/Ag^0 metal ratios was also obtained from analysis of edge positions in the XANES data (SI Fig. S8 and Table S2).

The stability and recyclability of a photocatalyst are important considerations in assessing the viability of a proposed technology. It has generally been assumed that the gradually decreasing activity of Ag@AgX materials in previously reported contaminant degradation studies was due to simple losses resulting from material transfer during the cyclic degradation experiments even though XRD showed an increase in the relative Ag^0 peak intensity [42–44]. EXAFS-LCF was used to monitor the change in Ag structure during the FA degradation studies described here with results demonstrating that Ag@AgCl/rGO also underwent continuous transformation to metallic Ag during contaminant degradation and not just during the synthesis process (Fig. 2 and Table S1). The catalyst recovered after 90 min, 120 min and 180 min degradation exhibited Ag^0 contents of 2.48%, 4.74% and 5.00%, respectively (increasing from 2.11% prior to use), while the non-oxygenated carbon content increased to 61% and 80%, respectively. These results indicate that continued decomposition of AgCl supported on rGO on photolysis occurred under the conditions of the studies described here.

The morphologies of the prepared photocatalyst samples were obtained by SEM, as shown in panels (a) to (e) in Fig. S6. It can be seen that the single composite particle was made up of irregularly shaped AgCl aggregates with sizes in the range of around 0.5–2.5 μm. Under different photoreduction conditions, the morphology of Ag@AgCl on rGO did not change markedly. Similarly, the recovered 90Ag@AgCl/rGO particles after formate degradation reaction were similar to those prior to formate degradation (see SI Fig. S7).

TEM of Ag@Ag/rGO hybrids also clearly illustrated that Ag@AgCl grains exhibited sizes in the range 0.2–0.5 micron and were closely anchored on the gauze-like GO sheets (panel (f), Fig. S6), however, it was difficult to reliably quantify the size distribution of Ag particles because the AgCl particles readily decomposed under the high energy electron beam.

N_2 sorption isotherms showed that both the photoreduced XAg@Ag/rGO catalysts and the recovered 90Ag@Ag/rGOY photocatalysts had very similar BET specific area values (Table 1). 30Ag@AgCl without rGO support exhibited the lowest BET specific area, most likely because severe aggregation occurred between the AgCl particles.

3.2. Impact of photoreduction time on the degradation of FA

The influence of photoreduction time on the photocatalytic decomposition of FA was examined for the as-prepared AgCl/GO (denoted as 0Ag@AgCl/rGO) and for AgCl/GO which was irradiated by visible light for different time periods in 50% ethanol solution under an argon atmosphere. The purpose of this photoreduction period was to partially reduce Ag^I present in AgCl to metallic Ag. Ag@AgCl/rGO mediated FA oxidation was followed for 120 min with the degradation observed to follow pseudo-first order kinetics over the first 60 min of degradation (Fig. 3). The pseudo-first order rate constant of FA oxidation for the various Ag@AgCl/rGO assemblages (which had been produced by photoreduction times of different durations) was determined by plotting $\ln([FA]/[FA]_0)$ versus time (t, min) and fitting a straight line to this data, with the pseudo-first order rate constant k' recovered as the slope of this line.

As can be seen from the results presented in Fig. 3, the duration of photoreduction significantly affected the activity of Ag@AgCl/rGO with respect to FA degradation. Of the seven XAg@AgCl/rGO catalysts prepared (X = 30, 60, 90, 120, 160, 200, 240 min, respectively), 90Ag@AgCl/rGO exhibited the highest photocatalytic activity with a degradation rate constant of 2.01 h^{-1}. In comparison, the degradation rate constants for 30Ag@AgCl/rGO, 60Ag@AgCl/rGO, 120Ag@AgCl/rGO and 240Ag@AgCl/rGO were 1.29 h^{-1}, 1.44 h^{-1}, 1.02 h^{-1} and 0.24 h^{-1}, respectively. The degradation rate constant for 90Ag@AgCl/rGO was almost eight times larger than that for 240Ag@AgCl/rGO, while the degradation rate constant for 60Ag@AgCl/rGO was slightly larger than that for 30Ag@AgCl/rGO. In addition, there was an apparent induction period for FA degradation over 0Ag@AgCl/rGO (see inset in Fig. 3), however, the rate of degradation of FA significantly increased after about 20 min. This implies that a certain amount of metallic Ag species is important for photocatalytic activity. Interestingly, while the degradation rate constant for the 30 min irradiated unsupported Ag/AgCl catalyst (1.20 h^{-1}) was slightly less than that of the rGO-supported catalyst 30Ag@AgCl/rGO irradiated for the same duration, the rate constant for degradation of FA by the unsupported Ag@AgCl catalyst is five times higher than that of 240Ag@AgCl/rGO which had been irradiated for 240 min. This suggests that once this initial effective Ag^0 content is achieved, extensive additional Ag(I) reduction leads to a significant decrease in performance.

It thus appears that a compromise of photoreduction time (for example, 90 min irradiation) to obtain both a certain content of Ag^0 particles and a particular extent of reduction of the GO support correlates with high photocatalytic activity. This finding is also consistent with the observation from previous studies that different photoreduction times led to both different amounts of metallic Ag formation through partial decomposition of AgCl and partial restoration of the graphene sp^2 carbon network under visible light irradiation [17,45,46].

On extended photolysis, excessive amounts of metallic Ag (for example, 8.40% Ag^0 in 240Ag@AgCl/rGO according to LCF-EXAFS

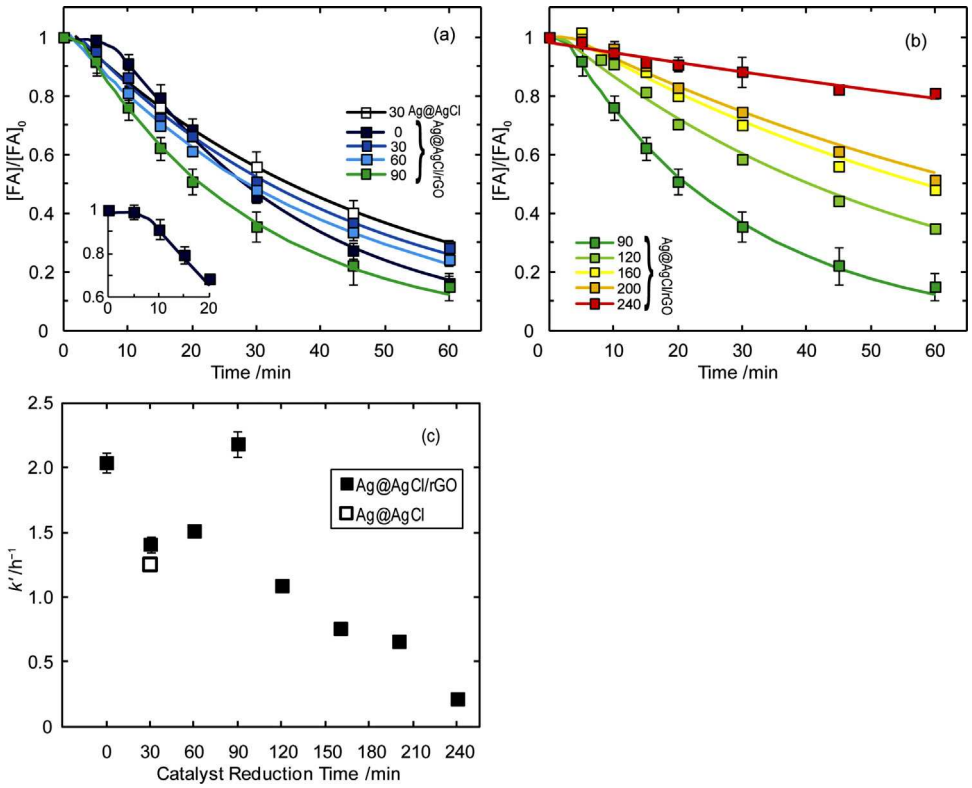

Fig. 3. Impact of photoreduction time upon activity of photocatalyst with respect to formate oxidation. Panel (a) and (b) show kinetic traces of formate oxidation runs as a function of the catalyst photo-reduction irradiation time for both Ag@AgCl/rGO and for Ag@AgCl. Symbols are the experimental data with solid lines demonstrating the fitted pseudo-first order decay functions, with an arbitrary smooth curve shown during the lag phase, if present. The inset illustrates the lag phase for the 0Ag@AgCl/rGO photocatalyst. Panel (c) shows the variation of the pseudo-first order rate constant for FA oxidation as a function of catalyst photoreduction time and support (data extracted from panels a and b). All experiments were conducted in duplicate in 10 mM NaCl, 2 mM $NaHCO_3$ at pH 8 with $[FA]_0 = 40\ \mu M$ and $0.5\ g\ L^{-1}$ photocatalyst.

analysis) formed on the AgCl grains. When the coverage of Ag^0 on AgCl increased beyond some optimal threshold value, a decrease in the rate constant for formate degradation was observed, with this decrease possibly associated with a decrease in availability of reactive sites for substrate adsorption or perhaps to some impact upon the primary photochemical process. The photocatalyst was also observed to turn black and aggregate at extended irradiation periods, presumably due to excessive metallic silver formation, a factor clearly detrimental to performance. A certain content of Ag^0 apparently promotes the separation of photogenerated electron–hole pairs and/or visible light harvesting through localized surface plasmonic resonance (LSPR) [47,48]. Nevertheless, too little Ag content resulted in insufficient active sites and ineffective inhibition of the recombination between photoproduced holes and electrons.

Although it is likely that 90Ag@AgCl/rGO (with 46% of oxygen bearing carbon, Table 1) only partially restored the π–π network, the increasing sp^2 carbon domains could presumably more effectively facilitate charge carrier separation. In comparison, without extensive light irradiation, the photocatalytic activity of 0Ag@AgCl/rGO showed distinctive degradation though with an induction period due (most likely) to insufficient Ag content and (possibly) defective sp^2 carbon domains in the reduced graphene oxide support.

3.3. Impacts of FA initial concentration and catalyst loading

The impact of varying the FA concentration at fixed Ag@AgCl/rGO loading as well as varying the Ag@AgCl/rGO loading at fixed FA concentration has been examined at pH 8 (Fig. 4). As can be seen from Fig. 4, the initial degradation rate for 5 μM FA ($6.5\ \mu M\ h^{-1}$) is almost seven times lower than that for 400 μM FA ($46.8\ \mu M\ h^{-1}$). The initial degradation rate of FA increased with increasing concentration of FA up to a concentration of 100 μM FA, at which point it reached a plateau and remained relatively constant at $\sim 50\ \mu M\ h^{-1}$ up to a concentration of 400 μM FA. This trend suggests that all incident photons are being captured by the catalyst and used to oxidize FA as fast as it can diffuse to the active sites, with a FA concentration of ~100 μM (under the conditions used here) sufficient for FA diffusion to match oxidant production. That is, at FA concentrations below 100 μM, oxidation rate would appear to be limited by the rate of diffusion of FA to oxidants at the catalysts surface while at higher concentrations the oxidation rate is most likely limited by photon flux.

The impact of catalyst loading (Fig. 5) was similar to the trend observed for FA concentration, namely, that the degradation rate of FA increased with higher catalyst amounts from $0.1\ g\ L^{-1}$ to $0.5\ g\ L^{-1}$ of 90Ag@AgCl/rGO, but then reached a plateau (note that different batches of catalyst were used for the FA concentration and catalyst concentration variation experiments, suggesting that the difference in maximal rate were likely due to inter-batch variability). The degradation rate for $1\ g\ L^{-1}$ of catalyst ($93.6\ \mu M\ h^{-1}$) is almost six times higher than that for the degradation of $0.1\ g\ L^{-1}$ of catalyst ($14.9\ \mu M\ h^{-1}$). However, further increase of catalyst loading to $2\ g\ L^{-1}$ led to a slightly lower degradation rate ($71.4\ \mu M\ h^{-1}$), which may be due to competition between FA and catalyst particles for the photo-formed oxidant.

3.4. Reactive oxidizing species measurement and trapping experiments

3.4.1. Impact of TBA on FA degradation

In order to probe the nature of the oxidizing species produced by Ag@AgCl/rGO, competition experiments were also

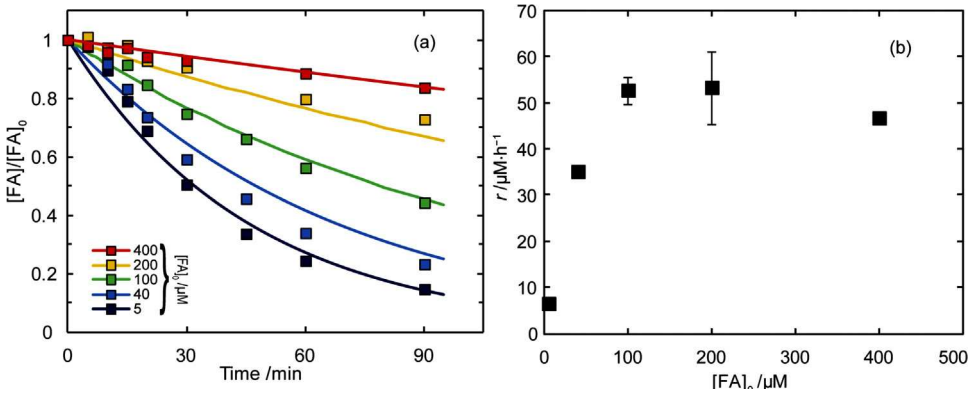

Fig. 4. Impact of initial FA concentration upon the FA degradation rate (initial FA concentrations as labelled in panel a). Panel (a) shows the kinetics observed for FA degradation, with symbols the average of duplicate experiments and solid lines the fitted pseudo-first order decay functions, whilst panel (b) demonstrates the initial formate oxidation rate (termed "*r*", as extracted from panel a) as a function of FA concentration. All experiments were conductedwith 0.5 g L^{-1} of 90Ag@AgCl/rGO in 100 mL of pH 8 buffer.

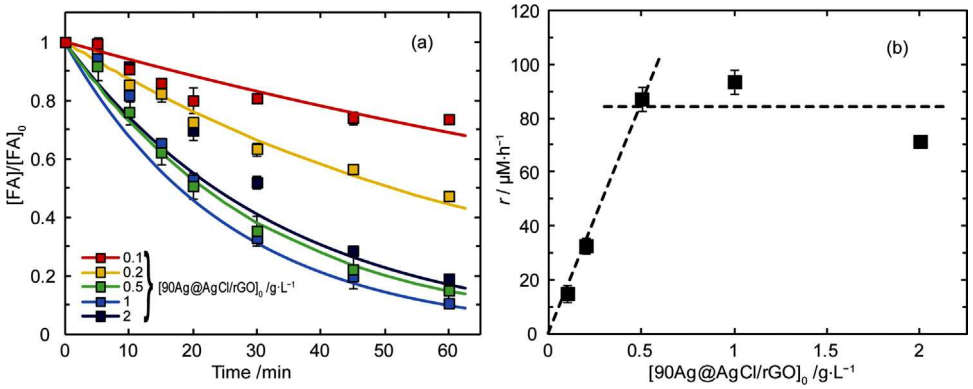

Fig. 5. Impact of catalyst loading (0.1–2 g L^{-1}) upon the initial degradation of FA. Panel (a) shows the kinetic traces of at least duplicate experiments, with the initial formate oxidation rate extracted from this data shown in panel (b). The solid lines in panel (a) are the fitted pseudo-first order decay functions, whereas the dashed lines in panel (b) are illustrative only. All experiments were conducted in pH 8 buffer with varying amounts of 90Ag@AgCl/rGO with $[FA]_0$ = 40 μM.

performed with varying amounts of TBA (Fig. 6). TBA reacts rapidly with powerful one electron oxidants such as HO• and Cl• ($k_{TBA+HO^\bullet} = 6 \times 10^8$ M^{-1} s^{-1} [49], $k_{TBA+Cl^\bullet} = 1.5 \times 10^9$ M^{-1} s^{-1} [50]) and, as such, should significantly retard FA oxidation if these species are involved. FA is also quite reactive with HO• ($k_{HCOO^-+HO^\bullet} = 3.2 \times 10^9$ M^{-1} s^{-1} [51]) and, although the rate constant for reaction of chlorine free radicals and formate ($k_{HCOO^-+Cl^\bullet}$) is not known, it is likely to be large when it is considered that $k_{HCOO^-+Br^\bullet} = 4.6 \times 10^8$ M^{-1} s^{-1} and $k_{CH_3COOH+Cl^\bullet} = 6 \times 10^8$ M^{-1} s^{-1} [50,52]. As such, TBA should readily compete with FA if Cl• or HO• are involved in the oxidation process.

Although interpretation of the TBA concentration study data is difficult given that the results obtained did not obey a simple competition equation, some deductions can still be made. Addition of TBA up to a concentration of 5 mM (i.e., [TBA] = 50 × [FA]) had a significant impact on the pseudo first order rate constant (Fig. 6) which, as expected, was observed to decrease with increasing TBA concentration. For concentrations of TBA ≤ 0.5 mM, the

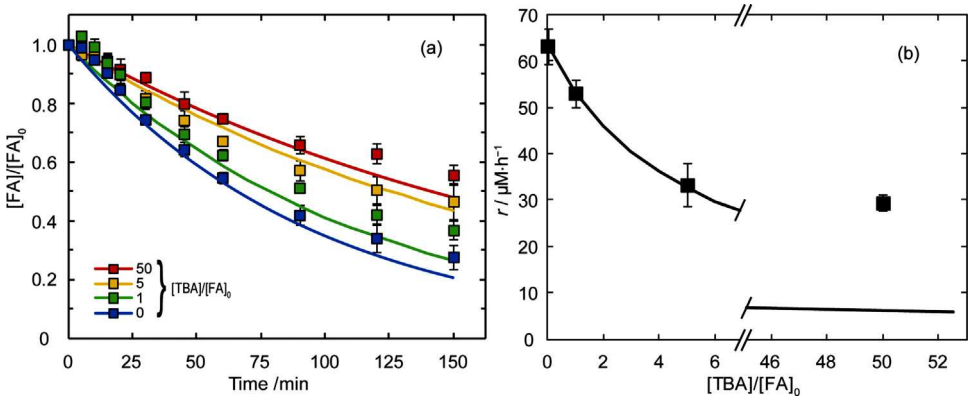

Fig. 6. Impact of TBA on the degradation of 100 μM FA. Panel (a) shows the kinetic traces as a function of TBA concentration, with symbols the experimental data and the solid lines the fitted pseudo-first order decay functions. Panel (b) demonstrates the variation of the initial formate degradation rate as a function of TBA concentration (data from panel (a)), with symbols the experimental data and the solid line a competition equation fitted to the data at $[TBA]/[FA]_0 \leq 5$ mM. All experiments were conducted with 0.5 g L^{-1} of 90Ag@AgCl/rGO in 100 mL of pH 8 buffer.

magnitude of this decrease was consistent with that expected if freely-diffusing HO• was the reacting species, however, at greater TBA concentrations the decrease in FA oxidation rate was much lower than would be expected if HO• was important; at a TBA concentration of 5 mM, an inhibition in FA oxidation rate of ~90% would be expected compared with the observed decrease of only ~50%. Although the TBA data suggest the importance of a fairly strong oxidant, they are inconclusive as to the nature of this species.

3.4.2. HO• measurement using phthalhydrazide

The involvement of HO• in AgX photocatalytic processes is still controversial. In view of the extremely high reactivity of HO• with solute species and the expected short diffusion distance from the catalyst surface, HO• is generally measured by indirect trapping methods, e.g. hydroxylation of aromatic compounds (e.g. terephthalic acid [53]) or formation of hydroxyl radical spin trap adducts [54]. However, these probes generally suffer from the inability to discriminate between HO• in bulk solution ($HO^{\bullet}_{aq}$) and surface bound HO• ($HO^{\bullet}_{surface}$). In addition, the adsorption and absorption of chemical probes and their by-products can significantly affect the measurement, therefore it is important to carefully consider these aspects when interpreting results. In this work we have applied a phthalhydrazide (Phth) chemiluminescence method to quantify the rate of production of HO•, with this method previously applied in both homogeneous systems [33] and in heterogeneous photocatalysis [55,56]. Reaction of HO• with Phth forms 5-hydroxy-2,3-dihydro-1,4-phthalazinedione (5-HO-Phth) in approximately 20% yield with this product emitting strong chemiluminescence when oxidized (e.g. by Cu(III)/H_2O_2) under alkaline conditions. This simple trap and trigger chemiluminescence method has previously been shown to be relatively insensitive to a range of interferences likely to be encountered including $HO_2^{\bullet}$ and $CO_3^{\bullet-}$ [55].

Phth interacted relatively strongly with the catalyst with ~15–20% adsorbing to the catalyst surface in the dark. Upon commencement of irradiation, the solution phase Phth concentration decreased from ~85% to ~75% of the initial added concentration (as determined from the UV absorbance of Phth in 0.22 μm filtered samples, see Fig. 6). These observations demonstrate that Phth should be able to probe both surface bound and freely-diffusing HO•, and suggest that Ag@AgCl/rGO is indeed capable of degradation of Phth. Although Phth was degraded during the irradiation, there was no increase in chemiluminescence, which in fact decreased with time (Fig. 7). As control experiments (described in the SI) have demonstrated that 5-HO-Phth is near-quantitatively recovered from Ag@AgCl/rGO catalyst suspensions, this absence of chemiluminescence increase strongly suggests that 5-HO-Phth is not formed in this system, thereby strongly refuting significant production of HO• in this system.

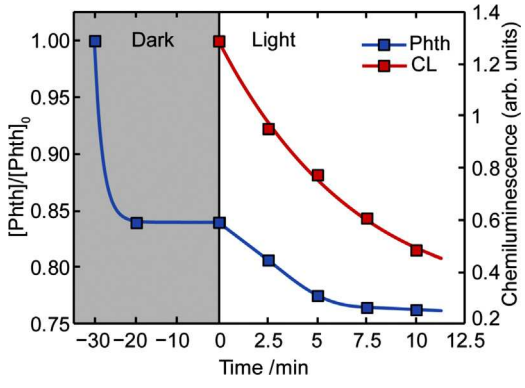

Fig. 7. Impact of adsorption and degradation on Phth concentration (left axis) as well as impact of irradiation upon chemiluminescence intensity (right axis). In the dark, Phth is rapidly adsorbed, and upon commencement of illumination at $t = 0$ seemingly degraded, with a concomitant decrease in chemiluminescence of the filtered reaction solution also observed, suggesting no 5-HO-Phth production. The reaction was performed with 0.5 g L^{-1} 90Ag@AgCl/rGO photocatalyst with $[Phth]_0 = 0.5$ mM in pH 8 10 mM NaCl, 2 mM $NaHCO_3$ solution. Symbols are experimental data with lines for illustrative purposes only.

3.4.3. Measurement of hypochlorite and hydrogen peroxide

Many recent reports claim that Ag@AgX and supported AgX catalysts are fairly stable and efficient, with several researchers suggesting that the gradual loss of photocatalytic activity during recycling experiments is due to the loss of photocatalyst during material transfer rather than possible intrinsic photocorrosion. However, the partial decomposition of AgCl would appear to be unavoidable because the combination of lattice silver cations with photogenerated electrons is likely significantly faster than the transfer of electrons to electron sinks such as Ag^0 or O_2 given the relatively long migration path [57,58]. The photocorrosion process results in holes being trapped by lattice Cl^-, presumably to yield $Cl^{\bullet}$, which could conceivably yield Cl_2 (and its hydrolysis products HClO and ClO^-, known as total free chlorine); similarly, should O_2 outcompete lattice Ag^+ for e^-, $O_2^{\bullet-}$ would be formed, which would disproportionate to yield H_2O_2. Therefore, analyses were undertaken for the potentially generated long-lived products total free chlorine and hydrogen peroxide using the DPD-spectrophotometric method [59,60].

It can be seen from Fig. 8 that the concentration of total free chlorine increased rapidly to about 2.5 μM during the first 10 min of irradiation and then gradually declined. This implies that total free chlorine does not accumulate to any significant extent and is unlikely to be of any relevance to substrate oxidation, although it does suggest that $Cl^{\bullet}$ is likely formed. In contrast, the concentration of H_2O_2 is far less than the method detection limit (0.2 μM). This result suggests that H_2O_2 does not accumulate in the system, precluding its significance as a direct oxidant. The absence of measurable H_2O_2 may also suggest that either $O_2^{\bullet-}$ is not formed, that $O_2^{\bullet-}$ is formed but rapidly reduces lattice Ag^+ to Ag^0, that $O_2^{\bullet-}$ is formed and able to "charge" AgNPs [61], or perhaps that H_2O_2, once formed, reacts rapidly with HOCl/OCl^- to produce $^1O_2$ [62].

4. Possible mechanism

Many mechanisms have been proposed to explain the photocatalytic behaviour of Ag@AgX based materials. Calzaferri and

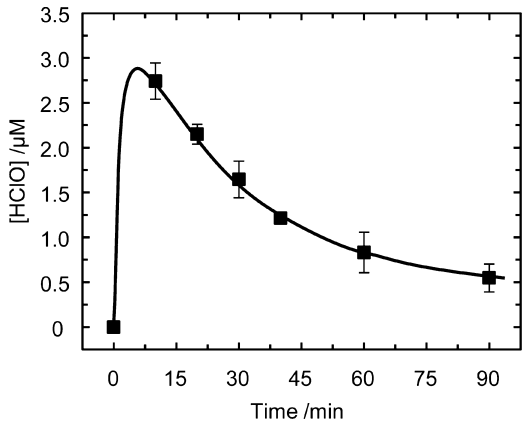

Fig. 8. Concentration of HClO/ClO^- formed upon irradiation of 1 g L^{-1} of 90Ag@AgCl/rGO photocatalyst in pH 8 10 mM NaCl, 2 mM $NaHCO_3$ solution. Symbols are averages of duplicate experiments with the solid line for illustrative purposes only.

coworkers [63,64] have suggested that the presence of small silver clusters at the AgCl surface reduces the effective band gap of the semiconductor as the silver clusters have empty energy levels below the energy of the AgCl conduction band. In the absence of silver clusters, AgCl does not absorb light below the indirect band gap transition of 3.3 eV (380 nm). The presence of the Ag clusters however is suggested to enable a new electronic transition from the AgCl valence band to the empty silver cluster energy levels with the holes remaining in the valence band as a result of this new visible wavelength induced transition available to initiate oxidation reactions [63]. Other investigators [22,45] have suggested that absorption of light by Ag^0 nanoparticles (as a result of the localized surface plasmon resonance (LSPR) of these particles) results in rapid injection of these electrons into the conduction band of the associated AgCl semiconductor with rapid transport of these electrons to the semiconductor surface where they may either initiate reduction reactions or, in the case of an rGO supported system, transfer to the conducting support material [65]. It is suggested that "hot holes" excited by the decay of surface plasmon resonance react with Cl ions in the outermost layers of the AgCl semiconductor producing highly oxidizing Cl atoms [64].

It has previously been suggested that the total mineralization of methyl orange by CNT/Ag/AgBr is very limited as a result of the formation of refractory reaction intermediates [66]. For example, formic acid is recognized as one possible intermediate preventing total mineralization [67]. As a strong electron donator ($E^0(CO_2/CO^{\bullet-}_2)) = -1.9$ V vs. NHE)), the $CO^{\bullet-}_2$ generated by photo-produced holes of AgCl could potentially inject supplementary electrons into the CB of AgCl to form a supplementary silver atom, since the combination of Ag^+ associated with an atom (Ag_2^+) or a cluster (Ag_n^+) is likely to be more rapid than the process of charge transfer [68]. Gradually, more metallic AgNPs would be expected to be generated.

$$HCOO^- + h^+ \rightarrow CO_2^{\bullet-} + H^+$$

$$CO_2^{\bullet-} + Ag_n^+ \rightarrow CO_2 + Ag_n$$

When supported on band gap matching graphene derived carbon materials, photogenerated electrons may efficiently transfer to the surface of supports thereby competitively retarding the fast recombination of charge carriers. As noted earlier, adsorbed electron acceptors such as oxygen are also typically assumed to react with photo-generated electrons (giving $CO_2^{\bullet-}$, H_2O_2, etc). Strongly adsorbed readily-reduced dyes (such as rhodamine B) may also act as efficient electron acceptors as they are also readily reduced ($k_{RhB+e(aq)^-} = 2.2 \times 10^{10}$ M^{-1} s^{-1} [69]). This process may explain why significant photocatalytic recycling has been observed when such dyes are used as substrates, whereas target compounds that are not readily reduced, such as formate, lead to gradual photocatalyst deactivation. Besides the oxidation by holes on AgCl or Ag_n^+, the generated $CO^{\bullet-}_2$ desorbed from the catalyst surface can also react with dissolved oxygen to produce CO_2 ($k = 4.2 \times 10^9$ M^{-1} s^{-1} [26]).

$$CO^{\bullet-}{}_2 + O_2 = CO_2 + O^{\bullet-}{}_2$$

In addition, partially restored graphene sheets anchor Ag@AgCl particles thereby preventing their aggregation and increasing the specific surface area (Table 1), however, the residuals of oxygen-bearing groups may also act as hole scavengers and compete with FA for these oxidants. rGO sheets contain ionisable carboxylic groups ($pK_a \sim 8$ [70]) which are likely to be at least partially ionized under our conditions (pH 8). As a result, repulsion of negatively-charged FA is expected, with adsorption on the rGO sheets expected to be negligible (which is also confirmed by the lack of quantifiable adsorption during the dark equilibration phase of the experiments). While the AgCl particles with a point of zero charge $pCl_{pzc} = 5.2$ are negatively charged at the pH of 8 used here, recalcitrant organic compounds such as formate and oxalate, both also negatively charged, would perhaps interact more strongly with the AgNP potentially affecting the stability, durability and activity of Ag@AgCl composites.

For the AgCl semiconductor, the calculated band gap energy (E_g) is 3.25 V, the conduction band minimum (CBM) is −0.06 V vs NHE and the valence band maximum (VBM) is 3.2 V vs. NHE [71]. Therefore the conduction band electrons in AgCl are not thermodynamically favourable for reduction of oxygen to superoxide as $E^0\left(O_2/O^{\bullet-}_2\right) = -0.16$ V vs. NHE [4]. As photogenerated electrons from AgNPs can transfer electrons to the CB (−0.2 V, vs NHE) of anatase TiO_2 under visible-light irradiation, it is believed that the plasmon-induced electrons of AgNPs and electrons transferred from the AgCl conduction band can easily transfer to the conduction band of rGO owing to the strong interaction between the interface of Ag@AgCl particles and the rGO nanosheets thereby lowering the electron–hole pair recombination rate and enhancing photocatalytic activity [18]. However, as the presence of the rGO support did not greatly enhance the performance of 30Ag@AgCl relative to 30Ag@AgCl/rGO (Fig. 1b), it is difficult to assess whether this process contributes to FA degradation under the conditions described here.

It is perhaps possible that the photogenerated electrons are transferred to the rGO support, reducing some functionalities on the support or undergoing additional processes. As it is typically assumed that O_2 will be the sink for the reducing equivalent from electron–hole pair formation, this raises the important question of what happens to this reducing equivalent. The results from this study suggest that in the absence of a readily reduced substrate, a significant fate of this electron is the reduction of Ag^+ within the catalyst as well as reduction of the rGO support, both processes which are shown here to negatively impact catalyst performance.

It is fair to conclude that, due to the complexity of a catalyst system involving heterojunctions between three materials (Ag^0, AgCl(s), and rGO), the underlying mechanism of photocatalytic contaminant oxidation by the graphene-supported Ag@AgCl composites used is still largely unresolved.

5. Conclusions

Visible light irradiation of Ag@AgCl/rGO assemblages has been shown here to result in simultaneous reduction of Ag^I present in AgCl to Ag nanoparticles and reduction in the oxygen-bound carbon content of the graphene support. While the carbon-based support undoubtedly assisted in preventing aggregation of the Ag@AgCl assemblages, there was little evidence of dramatic enhancement in oxidative ability due to the presence of the support material. The photoreduction time greatly affects the degradation performance with Ag@AgCl/rGO (2.11% of Ag present as Ag^0) generated by 90 min visible light irradiation during particle synthesis giving the highest photocatalytic activity. While not conclusive, this result can most likely be attributed to the presence of an optimal Ag^0 content leading to more effective charge carrier separation and an enhanced SPR effect. Extended irradiation times lead to low photocatalytic activity which is correlated to increased metallic Ag^0 content (up to 8.42% of total Ag in these studies), suggesting that the AgCl particles are highly coated in Ag^0 and that this is deleterious to performance.

The Ag@AgCl/rGO assemblages are effective photocatalysts for formic acid mineralization with the catalyst loading and target FA concentration significantly affecting the degradation performance of the catalyst. The degradation rate of FA initially increases with both higher catalyst and FA amounts, although subsequently appears to reach a maximum degradation rate, likely limited by the incoming light flux.

Application of a DPD-spectrophotometric method demonstrated that total free chlorine (denoted as $HOCl/OCl^-$) is quickly generated, rapidly reaching a maximum concentration that then decreases with time, whereas H_2O_2 was found to be below the detection limit, with the low concentrations of both these species likely making them irrelevant to target species degradation. Phth trapping experiments also demonstrated no production of $HO^\bullet$ in this system, with TBA competition experiments confirming the non-involvement of $HO^\bullet$. Although a strong oxidant appears to be formed that is capable of degradation of reasonably refractory organics, the results suggest that holes on the surface of AgCl or AgNPs or perhaps $Cl^\bullet$, rather than $HO^\bullet$, are important for FA degradation and the catalyst operation more generally. However, the photodecomposition of AgCl and the rGO support appears to be unavoidable, at least under the conditions used here, suggesting the useful lifetimes of Ag@AgCl/rGO materials will be limited unless effective approaches to preventing Ag^I reduction by photogenerated electrons can be developed.

Acknowledgements

Funding provided through ARC Discovery Grant DP12010322 is gratefully acknowledged. The authors would also like to acknowledge the Mark Wainwright Analytical Centre UNSW, Daniel D. Boland and Di He for their support on XAS measurements. XAS measurements were performed on the XAS beamline at the Australian Synchrotron under proposal numbers 4940 and 6951. We acknowledge the beamline staff for provision of technical support.

References

[1] S. Malato, P. Fernández-Ibáñez, M.I. Maldonado, J. Blanco, W. Gernjak, Catalysis Today 147 (2009) 1.
[2] W.Y. Teoh, J.A. Scott, R. Amal, Journal of Physical Chemistry Letters 3 (2012) 629.
[3] A. Fujishima, K. Honda, Nature 238 (1972) 37.
[4] C. Chen, W. Ma, J. Zhao, Chemical Society Reviews 39 (2010) 4206.
[5] A. Currao, V. Raja Reddy, M.K. van Veen, R.E.I. Schropp, G. Calzaferri, Photochemical & Photobiological Sciences 3 (2004) 1017.
[6] K. Pfanner, N. Gfeller, G. Calzaferri, Journal of Photochemistry and Photobiology A: Chemistry 95 (1996) 175.
[7] P. Wang, B.B. Huang, X.Y. Qin, X.Y. Zhang, Y. Dai, J.Y. Wei, M.H. Whangbo, Angewandte Chemie International Edition 47 (2008) 7931.
[8] B. Tian, J. Zhang, Catalysis Surveys from Asia 16 (2012) 210.
[9] V. Singh, D. Joung, L. Zhai, S. Das, S.I. Khondaker, S. Seal, Progress in Materials Science 56 (2011) 1178.
[10] X. Huang, X. Qi, F. Boey, H. Zhang, Chemical Society Reviews (2012).
[11] Y. Zhu, S. Murali, W. Cai, X. Li, J.W. Suk, J.R. Potts, R.S. Ruoff, Advanced Materials 22 (2010) 3906.
[12] C. Xu, Y. Yuan, A. Cui, R. Yuan, Journal of Materials Science 48 (2013) 967.
[13] J. Wang, C. An, J. Liu, G. Xi, W. Jiang, S. Wang, Q.-H. Zhang, Journal of Materials Chemistry A 1 (2013) 2827.
[14] M. Zhu, P. Chen, M. Liu, Journal of Materials Chemistry 22 (2012) 21487.
[15] M. Zhu, P. Chen, M. Liu, Langmuir 28 (2012) 3385.
[16] M. Zhu, P. Chen, M. Liu, ACS Nano 5 (2011) 4529.
[17] H. Zhang, X.F. Fan, X. Quan, S. Chen, H.T. Yu, Environmental Science and Technology 45 (2011) 5731.
[18] G. Luo, X. Jiang, M. Li, Q. Shen, L. Zhang, H. Yu, ACS Applied Materials & Interfaces (2013).
[19] M.R. Hoffmann, S.T. Martin, W. Choi, D.W. Bahnemann, Chemical Reviews 95 (1995) 69.
[20] Y.P. Bi, J.H. Ye, Chemical Communications (2009) 6551.
[21] J. Jiang, L.Z. Zhang, Chemistry A European Journal 17 (2011) 3710.
[22] L. Ye, J. Liu, C. Gong, L. Tian, T. Peng, L. Zan, ACS Catalysis 2 (2012) 1677.
[23] Y.H. Ng, S. Ikeda, M. Matsumura, R. Amal, Energy & Environmental Science 5 (2012) 9307.
[24] O. Merka, V. Yarovyi, D.W. Bahnemann, M. Wark, Journal of Physical Chemistry C 115 (2011) 8014.
[25] T. Wu, G. Liu, J. Zhao, H. Hidaka, N. Serpone, The Journal of Physical Chemistry B 102 (1998) 5845.
[26] J. Krýsa, G. Waldner, H. Měšťánková, J. Jirkovský, G. Grabner, Applied Catalysis B: Environmental 64 (2006) 290.
[27] M.I. Franch, J.A. Ayllón, J. Peral, X. Domènech, Catalysis Today 76 (2002) 221.
[28] J. Sá, C.A. Agüera, S. Gross, J.A. Anderson, Applied Catalysis B: Environmental 85 (2009) 192.
[29] A. Tanaka, K. Hashimoto, B. Ohtani, H. Kominami, Chemical Communications 49 (2013) 3419.
[30] C.J. Miller, H. Yu, T.D. Waite, Colloids and Surfaces A: Physicochemical and Engineering Aspects (2013), in press.
[31] R. Prins, D.C. Koningsberger, X-ray Absorption: Principles, Applications, Techniques of EXAFS, SEXAFS, and XANES, New York Wiley, New York, NY, 1988.
[32] T. Ressler, Journal of Synchrotron Radiation 5 (1998) 118.
[33] C.J. Miller, A.L. Rose, T.D. Waite, Analytical Chemistry 83 (2010) 261.
[34] A. Ganguly, S. Sharma, P. Papakonstantinou, J. Hamilton, The Journal of Physical Chemistry C 115 (2011) 17009.
[35] A.K. Swain, D. Li, D. Bahadur, Carbon 57 (2013) 346.
[36] K.N. Kudin, B. Ozbas, H.C. Schniepp, R.K. Prud'homme, I.A. Aksay, R. Car, Nano Letters 8 (2007) 36.
[37] O. Akhavan, M. Abdolahad, A. Esfandiar, M. Mohatashamifar, The Journal of Physical Chemistry C 114 (2010) 12955.
[38] D.C. Kim, D.-Y. Jeon, H.-J. Chung, Y. Woo, J.K. Shin, S. Seo, Nanotechnology 20 (2009) 375703.
[39] S. Park, K.-S. Lee, G. Bozoklu, W. Cai, S.T. Nguyen, R.S. Ruoff, ACS Nano 2 (2008) 572.
[40] M. Koinuma, C. Ogata, Y. Kamei, K. Hatakeyama, H. Tateishi, Y. Watanabe, T. Taniguchi, K. Gezuhara, S. Hayami, A. Funatsu, M. Sakata, Y. Kuwahara, S. Kurihara, Y. Matsumoto, The Journal of Physical Chemistry C 116 (2012) 19822.
[41] A. Dimiev, D.V. Kosynkin, L.B. Alemany, P. Chaguine, J.M. Tour, Journal of the American Chemical Society 134 (2012) 2815.
[42] Y. Li, Y. Ding, The Journal of Physical Chemistry C 114 (2010) 3175.
[43] W. Cui, H. Wang, L. Liu, Y. Liang, J.G. McEvoy, Applied Surface Science 283 (2013) 820.
[44] Y. Tang, Z. Jiang, G. Xing, A. Li, P.D. Kanhere, Y. Zhang, T.C. Sum, S. Li, X. Chen, Z. Dong, Z. Chen, Advanced Functional Materials 23 (2013) 2932.
[45] Y. Matsumoto, M. Koinuma, S. Ida, S. Hayami, T. Taniguchi, K. Hatakeyama, H. Tateishi, Y. Watanabe, S. Amano, The Journal of Physical Chemistry C 115 (2011) 19280.
[46] X. Jiang, J. Nisar, B. Pathak, J. Zhao, R. Ahuja, Journal of Catalysis 299 (2013) 204.
[47] P. Wang, B. Huang, Y. Dai, M.-H. Whangbo, Physical Chemistry Chemical Physics 14 (2012) 9813.
[48] S. Linic, P. Christopher, D.B. Ingram, Nature Materials 10 (2011) 911.
[49] G.V. Buxton, C.L. Greenstock, W.P. Helman, A.B. Ross, Journal of Physical and Chemical Reference Data 17 (1988) 513.
[50] B.C. Gilbert, J.K. Stell, W.J. Peet, K.J. Radford, Journal of the Chemical Society, Faraday Transactions 1: Physical Chemistry in Condensed Phases 84 (1988) 3319.
[51] W.P. Kwan, B.M. Voelker, Environmental Science and Technology 36 (2002) 1467.
[52] G. Merenyi, J. Lind, Journal of the American Chemical Society 116 (1994) 7872.
[53] K.-i. Ishibashi, A. Fujishima, T. Watanabe, K. Hashimoto, Journal of Photochemistry and Photobiology A: Chemistry 134 (2000) 139.
[54] J. Jiang, H. Li, L. Zhang, Chemistry A European Journal 18 (2012) 6360.
[55] S. Backa, K. Jansbo, T. Reitberger, Holzforschung 51 (1997) 557.
[56] H. Liao, T. Reitberger, Catalysts 3 (2013) 418.
[57] Y.G. Xu, H. Xu, H.M. Li, J.X. Xia, C.T. Liu, L. Liu, Journal of Alloys and Compounds 509 (2011) 3286.
[58] T. Li, Y. He, H. Lin, J. Cai, L. Dong, X. Wang, M. Luo, L. Zhao, X. Yi, W. Weng, Applied Catalysis B: Environmental 138–139 (2013) 95.
[59] W.J. Cooper, N.M. Roscher, R.A. Slifker, Journal (American Water Works Association) 74 (1982) 362.
[60] H. Bader, V. Sturzenegger, J. Hoigné, Water Research 22 (1988) 1109.
[61] D. He, S. Garg, T.D. Waite, Langmuir 28 (2012) 10266.
[62] A.U. Khan, M. Kasha, Proceedings of the National Academy of Sciences of the United States of America 91 (1994) 12362.
[63] M. Lanz, D. Schürch, G. Calzaferri, Journal of Photochemistry and Photobiology A: Chemistry 120 (1999) 105.
[64] D. Schürch, A. Currao, S. Sarkar, G. Hodes, G. Calzaferri, Journal of Physical Chemistry B 106 (2002) 12764.
[65] C. Gómez-Navarro, R.T. Weitz, A.M. Bittner, M. Scolari, A. Mews, M. Burghard, K. Kern, Nano Letters 7 (2007) 3499.
[66] Y. Xu, H. Xu, J. Yan, H. Li, L. Huang, Q. Zhang, C. Huang, H. Wan, Physical Chemistry Chemical Physics 15 (2013) 5821.
[67] M. Stylidi, D.I. Kondarides, X.E. Verykios, Applied Catalysis B: Environmental 47 (2004) 189.
[68] J. Belloni, M. Treguer, H. Remita, R. De Keyzer, Nature 402 (1999) 865.
[69] E.A. Kucherenko, L.I. Kartasheva, A.K. Pikaev, High Energy Chemistry 16 (1982) 168.
[70] B. Konkena, S. Vasudevan, Journal of Physical Chemistry Letters 3 (2012) 867.
[71] J. Hou, Z. Wang, C. Yang, W. Zhou, S. Jiao, H. Zhu, Journal of Physical Chemistry C 117 (2013) 5132.